NeuroImage: Clinical 34 (2022) 103012

Contents lists available at ScienceDirect

NeuroImage: Clinical

journal homepage: www.elsevier.com/locate/ynicl

Periventricular magnetisation transfer abnormalities in early multiple sclerosis

Lukas Pirpamer [a], Bálint Kincses [b], Zsigmond Tamás Kincses [b,c], Christian Kiss [d], Anna Damulina [d], Michael Khalil [d], Rudolf Stollberger [e], Reinhold Schmidt [a], Christian Enzinger [d,f,*], Stefan Ropele [d]

[a] Department of Neurology, Division of Neurogeriatrics, Medical University of Graz, Austria
[b] Department of Neurology, Albert Szent-Györgyi Clinical Center, University of Szeged, Szeged, Hungary
[c] Department of Radiology, Albert Szent-Györgyi Clinical Center, University of Szeged, Szeged, Hungary
[d] Department of Neurology, Division of General Neurology, Medical University Graz, Austria
[e] Institute of Medical Engineering, Graz University of Technology, Graz, Austria
[f] Division of Neuroradiology, Interventional and Vascular Radiology, Department of Radiology, Medical University of Graz, Austria

ARTICLE INFO

Keywords:
Normal-appearing white matter
Magnetisation transfer ratio
Periventricular gradient
Cortical thinning
MRI
Multiple sclerosis

ABSTRACT

Objective: Recent studies suggested that CSF-mediated factors contribute to periventricular (PV) T2-hyperintense lesion formation in multiple sclerosis (MS) and this in turn correlates with cortical damage. We thus investigated if such PV-changes are observable microstructurally in early-MS and if they correlate with cortical damage.
Methods: We assessed the magnetisation transfer ratio (MTR) in PV normal-appearing white matter (NAWM) and in MS lesions in 44 patients with a clinically isolated syndrome (CIS) suggestive of MS and 73 relapsing-remitting MS (RRMS) patients. Band-wise MTR values were related to cortical mean thickness (CMT) and compared with 49 healthy controls (HCs). For each band, MTR changes were assessed relative to the average MTR values of all HCs.
Results: Relative to HCs, PV-MTR was significantly reduced up to 2.63% in CIS and 5.37% in RRMS ($p < 0.0001$). The MTR decreased towards the lateral ventricles with 0.18%/mm in CIS and 0.31%/mm in RRMS patients, relative to HCs. In RRMS, MTR-values adjacent to the ventricle and in PV-lesions correlated positively with CMT and negatively with EDSS.
Conclusion: PV-MTR gradients are present from the earliest stage of MS, consistent with more pronounced microstructural WM-damage closer to the ventricles. The positive association between reduced CMT and lower MTR in PV-NAWM suggests a common pathophysiologic mechanism. Together, these findings indicate the potential use of multimodal MRI as refined marker for MS-related tissue changes.

1. Introduction

Several magnetisation transfer ratio (MTR) studies in multiple sclerosis (MS) patients have reported an abnormal gradient towards the ependyma of the lateral ventricles (Brown et al., 2020; 2017; Liu et al., 2015; Pardini et al., 2016; Poirion et al., 2021; Samson et al., 2014). The MTR is based on the energy exchange between tissue water and the subcellular tissue matrix through various mechanisms including dipolar coupling and chemical exchange. Reduced MTR values are the consequence of a reduction of macromolecular bound protons and are therefore considered as a measure of microstructural tissue damage (Ropele and Fazekas, 2009). The observation of a MTR gradient in periventricular (PV) normal-appearing white matter (NAWM) has been suggested to be compatible with the concept of inflammation through CSF-derived soluble factors which have been proposed to cause or mediate activation of microglia, adding to the disease activity in MS (Lassmann, 2014; Magliozzi et al., 2010; Storch et al., 2006). While the pathophysiological mechanisms are not clear yet, a recent positron emission tomography (PET) study with a fluorinated translocator protein (TSPO) tracer has demonstrated a gradient of innate immune cell

* Corresponding author at: General Neurology incl. Stroke-Unit, Head Multiple Sclerosis Outpatient Clinic, University Clinic of Neurology, Auenbruggerplatz 22, A-8036 Graz, Medical University of Graz, Austria.
E-mail address: chris.enzinger@medunigraz.at (C. Enzinger).

https://doi.org/10.1016/j.nicl.2022.103012
Received 30 August 2021; Received in revised form 14 April 2022; Accepted 18 April 2022
Available online 20 April 2022

activation running parallel to the MTR gradient (Poirion et al., 2021).

However, MTR variations around the lateral ventricles can also be observed in normal brains (Pardini et al., 2016) and MTR is globally reduced in NAWM of MS patients (Filippi et al., 1995). Of note, such a gradient has been demonstrated mostly in established MS with longer disease duration and in progressive forms of MS so far (Brown et al., 2020; Liu et al., 2015; Pardini et al., 2016; Poirion et al., 2021). Hitherto, only a single study has addressed the question if the gradient is also present from the earliest clinical stage of MS (Brown et al., 2017). This investigation found that patients with a clinically isolated optic neuritis had lower periventricular MTR values than healthy controls (HCs), and that those patients who had a steeper MTR gradient had a higher probability to develop clinically definite MS within the next 2-years. However, the researchers did not assess MTR in clinically definite MS patients and restricted the MTR analysis to just two axial slices to minimize partial volume effects.

The aim of our cross-sectional study thus was first to probe for such an MTR gradient in a cohort of patients with a clinically isolated syndrome (CIS) suggestive of MS and to compare it with clinically definite MS patients and HCs. Second, in order to scrutinise the possibility of

Table 1
Demographical data of subjects and descriptive statistic.

Variables	HCs	MS patients	CIS	RRMS	MS vs. HC		CIS vs. HC		RRMS vs. HC				RRSM vs. CIS
	(n = 49)	(n = 117)	(n = 44)	(n = 73)	PD (%)	p-value	PD (%)	p-value	PD (%)	p-value		PD (%)	p-value	
Demographics														
Age (years): mean (SD)	28.5 (6.5)	32.6 (8.6)	33.2 (8.9)	32.3 (8.5)	+14	0.004	[a]	+16	0.004	[a]	+13	0.01	[a]	−2.8	0.577	[a]
Sex (female/male)	40/9	79/38	31/13	48/25	−17	0.067	[b]	−13	0.21	[b]	−19	0.057	[b]	−6.7	0.603	[b]
Clinical parameters														
dDisease duration (months): median (IQR)	na	8.0 (2.0; 78.5)	3.0 (1.0; 6.0)	51.0 (3.8; 115.5)	na	na		na	na		na	na		+1600	<0.0001	[b]
EDSS: median (IQR)	na	1.5 (1.0; 2.0)	1.0 (0.0; 2.0)	2.0 (1.0; 2.5)	na	na		na	na		na	na		+100	0.004	[b]
MR volumetry														
Brain volume (normalized) (ml): median (IQR)	1163.8 (39.5)	1154.3 (54.1)	1166.4 (49.4)	1147.1 (55.9)	−0.8	0.268	[b]	+0.2	0.783	[b]	−1.4	0.072	[b]	−1.7	0.129	[b]
CSF volume (normalized) (ml): median (IQR)	19.4 (16.5; 23.0)	21.0 (16.4; 29.3)	19.8 (17.6; 22.6)	23.2 (15.6; 30.6)	+8.2	0.143	[b]	+2.3	0.551	[b]	+19	0.079	[b]	+17	0.349	[b]
Cortical mean thickness (normalized) (mm): mean (SD)	2.6 (0.1)	2.4 (0.2)	2.5 (0.1)	2.4 (0.2)	−4.4	<0.0001	[a]	−3.9	<0.001	[a]	−4.7	<0.0001	[a]	−0.9	0.456	[a]
LL volume (ml): median (IQR)	na	6.0 (3.1; 13.8)	4.6 (2.8; 11.1)	7.3 (3.2; 21.9)	na	na		na	na		na	na		+60	0.032	[b]
PV-LL volume (ml): median (IQR)	na	2.6 (0.8; 7.8)	2.0 (0.1; 5.4)	3.2 (1.4; 14.8)	na	na		na	na		na	na		+60	0.015	[b]
non PV-LL volume (ml): median (IQR)	na	2.9 (1.4; 5.9)	2.4 (0.6; 4.7)	3.4 (1.6; 7.2)	na	na		na	na		na	na		+42	0.031	[b]
PV-LL% (%): mean (SD)	na	48.5 (27.8)	44.2 (32.1)	51.0 (24.8)	na	na		na	na		na	na		+15	0.208	[a]
MTR in lesions														
MTR in PVL (ratio): mean (SD)	na	0.313 (0.023)	0.313 (0.023)	0.313 (0.023)	na	na		na	na		na	na		−0.038	0.98	[a]
MTR in non-PVL (ratio): mean (SD)	na	0.340 (0.021)	0.340 (0.021)	0.339 (0.021)	na	na		na	na		na	na		−0.294	0.81	[a]

[a]Student's T-Test;
[b]Mann-Whitney U;
na = not applicable; PD = percentage difference;
EDSS = Expanded Disability Status Scale, MTR = magnetisation transfer ratio, CSF = cerebrospinal fluid, LL = white matter lesion load, PV = *peri*-ventricular, PV-LL% = percentage of periventricular lesion load, NAWM = normal-appearing white matter, SD = standard deviation, IQR = inter quartile range, HCs = healthy controls, MS = multiple sclerosis, CIS = clinically isolated syndrome, RRMS = relapsing-remitting MS.

potential common pathophysiological factors in these different compartments of the brain, we assessed linked effects in periventricular regions and in the cerebral cortex by measuring cortical thickness, based on the fact that the outer layers of the cortex are also close to CSF and have been linked to meningeal inflammation (Magliozzi et al., 2010; Serafini et al., 2004). We therefore hypothesised that beyond focal T2 hyperintense periventricular lesions (Jehna et al., 2015), also *microstructural* MTR changes are associated with cortical damage in this specific group of patients with early MS.

2. Material and methods

2.1. Subjects

In this retrospective study, brain MRI scans from 120 patients (81 females, 39 males, mean age = 32.4 +/-8.7) were included (median EDSS = 1.5, IQR = [1.0; 2.0]), of which were 46 CIS (median EDSS = 1.0, IQR = [0.0; 2.0]) and 74 relapsing-remitting MS (RRMS) patients (median EDSS = 2.0, IQR = [1.0; 2.5]). All CIS and RRMS patients were diagnosed according to the 2010 McDonald criteria (Polman et al., 2011). Neurological disability was assessed using the Expanded Disability Status Scale (EDSS) (Kurtzke, 1983). Additionally, 49 HCs (40 females, 9 males, mean age = 28.5 +/-6.5 years) without neurological deficit were scanned with the same MRI protocol. All HCs underwent a structured history taking and a neurologic exam by board certified neurologists. The healthy participants did not have any concomitant neurological or psychiatric disease and none of them took medication. The local ethics committee had approved the study and each participant gave written informed consent. Patient characteristics are listed in Table 1. After visual inspection of the MRI examinations, three subjects had to be excluded due to motion artefacts during the MT-weighted image acquisition.

2.2. MRI acquisition

Imaging was performed on a 3T Tim-Trio system (Siemens Medical Systems, Erlangen, Germany) using a 12-element head coil. High-resolution images were obtained using a T1-weighted magnetisation prepared rapid gradient-echo sequence (MPRAGE, TR/TE/TI = 1900/2.19/900 ms) with 1 mm-isotropic resolution. To identify and segment hyperintense MS lesions, T2-weighted FLAIR images were acquired (TR/TE/TI = 10000/69/2500 ms) with 0.9x0.9 mm^2 in-plane resolution and 3 mm slice-thickness. MT imaging was implemented with two spoiled 3D gradient-echo sequences (TR = 40 ms, TE = 7.38 ms, flip-angle = 15°, number of slices = 40, slice-thickness = 3 mm, in-plane resolution = 0.9 × 0.9 mm) which were consecutively performed with and without a Gauss-Hanning-shaped MT saturation pulse (off-resonance-frequency = 1.2 kHz, FA = 500°, duration = 9984us).

2.3. MRI data processing

For MTR mapping, both gradient-echo sequences (with MT contrast (MTC) and without the MT pulse (noMTC)) were rigidly co-registered using FSL-FLIRT (https://fsl.fmrib.ox.ac.uk/). MTR was calculated with the following formula: MTR = (noMTC–MTC)/noMTC.

Semiautomatic segmentation of MS lesions (located in PV, deep and juxtacortical WM) was performed on T2w-FLAIR images by a trained operator, selecting a conservative approach disregarding lesions below a size of 3 mm, as described earlier (Jehna et al., 2015). Cortical and infratentorial lesions were not assessed in the current study. FLAIR and MT-weighted images were rigidly co-registered to the high-resolution T1-MPRAGE sequence using *flirt* (part of FSL) with six degrees of freedom. Lesion masks were transformed by the resulting transformation matrices, using trilinear interpolation and a threshold of 50%. Brain volumetry, including measurement of cortical thickness, and regional segmentation was performed with FreeSurfer (v6.0 https://surfer.nmr.mgh.harvard.edu/) on the 1 mm-isotropic T1-sequence. A ventricle mask, which successively was used to generate ventricle margins, was generated by merging the FreeSurfer-processed lateral ventricle masks, the 3rd and 4th ventricle and the CSF mask. Cortical mean thickness (CMT) was normalized by the cubic root of intracranial volume.

2.4. Measurement of MTR in periventricular and non-periventricular lesions

PV-lesions (PVL) and non-PVL were classified by an in-house developed MATLAB (https://www.mathworks.com/) algorithm as described earlier (Jehna et al., 2015). In brief, a ventricle margin was created by dilating the ventricle mask by three voxels in all three-dimensions. Lesions containing common voxels with the ventricle margin were classified as PVL. The remaining lesions were identified as non-PVL. Averaged MTR values were calculated in PV and non-PVL using *fslstats* (part of FSL).

2.5. Assessment of MTR in NAWM-bands around the ventricle

To assess MTR changes in NAWM as a function of distance from ventricular CSF, ten equidistant bands were computed by an iterative dilation of the ventricle mask by one voxel and finally by multiplying the bands with the FreeSurfer-segmented global white-matter (WM)-mask (Fig. 1B). To ensure that NAWM-bands did not contain lesions, all lesions were dilated by 5 mm and any overlapping voxels with the WM-bands were excluded from the analysis (Fig. 1C). To account for segmentation imperfections and to reduce the influence of partial volume effects with CSF, the band at 1 mm distance was excluded from further analyses, thus the first band was defined at 2 mm distance.

Averaged MTR values were computed for MS patients and HCs in each band. To assess the relative MTR reduction for each band in MS patients, we computed an average MTR value for all HCs and calculated a percentual deviation for each MS patient. This procedure is expressed in the following formula, where *s* stands for an MS-subject and *b* for one of the ventricle bands.

$$relMTR_{s,b} = \left(1 - \frac{MTR_{s,b}}{mean\left(MTR_{HC,b}\right)}\right) \cdot 100$$

In contrast to previous studies that calculated the MTR gradient by the difference of two margins only (Brown et al., 2020; 2017; Liu et al., 2015; Pardini et al., 2016), we calculated the MTR-gradient by the percentual MTR reduction relative to the average MTR values of HCs in each band and by fitting a regression line through all margins using linear fit with robust bi-squares weighting in MATLAB.

2.6. Parameter estimates and statistics

Statistical analyses were performed with RStudio (v1.3.1093 https://www.r-project.org/). Differences between CIS, RRMS, and HCs were calculated by Student's *T*-Test for normally distributed data or by Mann-Whitney-*U* test in case of nonparametric distribution, which was determined using the Lilliefors-Test.

To study the relationships between CMT and periventricular MTR values as well as the association with EDSS, Pearson (r_P) or Spearman (r_S) correlation analyses were applied. P-values < 0.05 were considered statistically significant. Given the explorative nature of the study, no correction for multiple comparisons was employed.

3. Results

The demographic data of all subjects are summarized in Table 1. There were no significant demographic differences between the CIS and RRMS cohort. RRMS patients had a significantly longer median disease

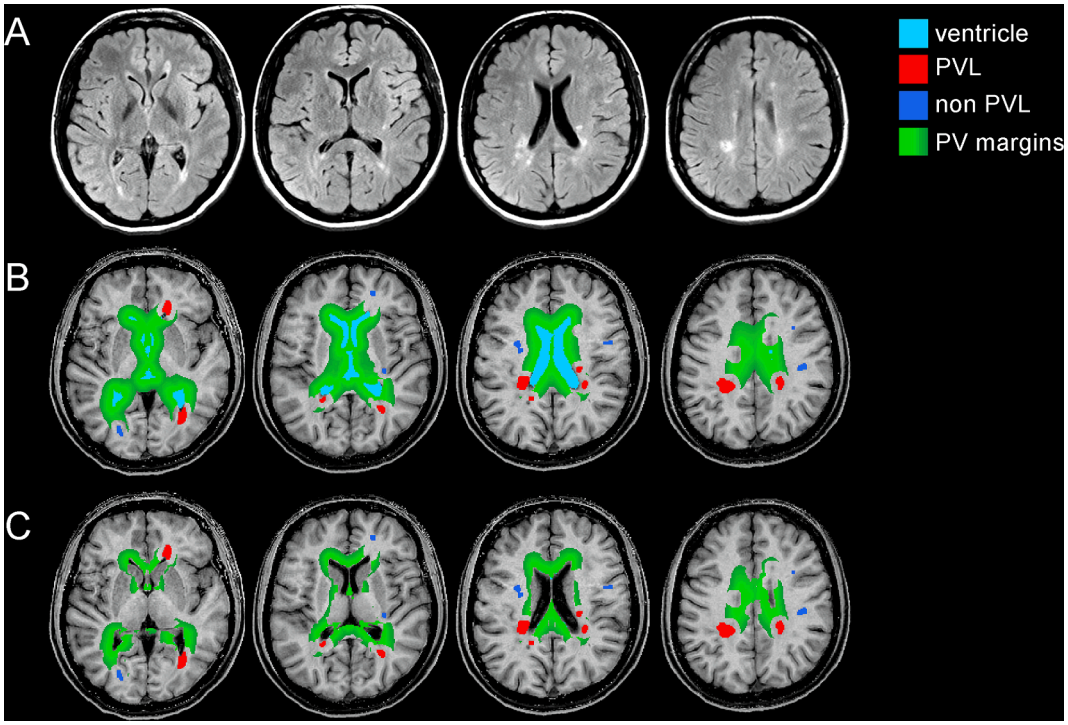

Fig. 1. Exemplary segmentation results of periventricular lesions (red), non-periventricular lesions (dark blue), ventricle-segmentation (light blue) and periventricular margins (green shades). All lesions are surrounded by a 5-voxel security margin that was also not considered as normal-appearing white matter (NAWM). **(A)** FLAIR images registered to the isotropic T1 space (please note, that due to the application of the registration-transformation on the binary segmented WMH-masks, small lesions might not appear properly segmented on the registered image). **(B)** Original segmentation in three horizontal slices of the brain at different levels; **(C)** final segmentation of PV margins in NAWM after multiplication with the global WM-mask. FLAIR = fluid attenuated inversion recovery, WMH = white matter hyperintensities, NAWM = normal appearing white matter.

duration (51 months) compared to CIS (3 months) along with a higher EDSS (2.0 vs 1.0). Brain volumetry revealed no differences between the normalized brain or ventricle volumes between groups (Table 1). Normalized CMT was reduced in CIS and RRMS compared to HCs, but did not significantly differ between CIS and RRMS patients. The total hyperintense WM lesion-load was 60% higher in RRMS than in CIS (7.3 ml vs 4.6 ml, p = 0.032), and the PV lesion-load was also 60% increased (3.2 ml vs 2.0 ml, p = 0.015). The increase was less pronounced in non-PVL (+42%), but it was still statistically significant (3.4 ml vs 2.4 ml, p = 0.031) (Table 1). Non PVL lesions were primarily located in deep WM and only a small portion of these lesions were located juxtacortically. We did not observe any cases with diffusely abnormal white matter (DAWM; also called "dirty white matter") on FLAIR images.

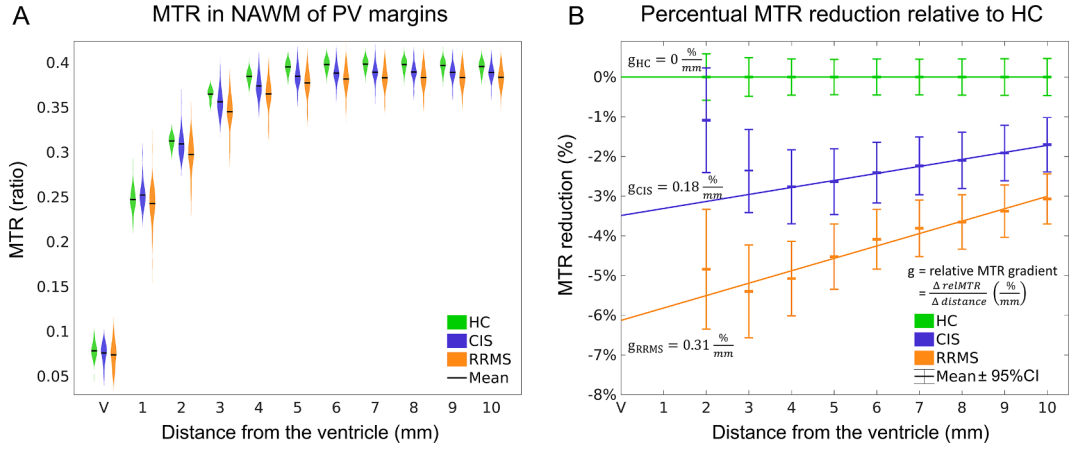

Fig. 2. **A:** Violin plots of mean magnetization transfer ratio (MTR) values as a function of the distance from the ventricle (V) in the NAWM in healthy controls (HCs), clinically isolated syndrome (CIS) and relapsing-remitting multiple sclerosis (RRMS) patients. **B:** Percentual reduction of MTR in CIS (blue) and RRMS (orange) relative to mean MTR values of HCs (green) in each band. Regression lines are fitted between 4 mm and 10 mm distance to reduce the influence of partial volume effects. The resulting slopes (relative MTR gradient) were 0.18%/mm in CIS and 0.31%/mm in RRMS patients. Please note, the linear approximation of the relative MTR decrease does only represent the decrease in the periventricular zone and cannot be extrapolated for the entire brain. MTR = magnetisation transfer ratio, NAWM = normal-appearing white matter, PV = peri ventricular, HCs = healthy controls, CIS = clinically isolated syndrome, RRMS = relapsing-remitting multiple sclerosis, CI = confidence interval.

3.1. MTR in periventricular and non-periventricular lesions

While MTR values in PVL and non-PVL did not differ between groups (group-wise average of MTR in PVL: CIS = 0.313, RRMS = 0.313, p = 0.980; non-PVL: CIS = 0.340, RRMS = 0.339, p = 0.810; Table 1), MTR values in PVL generally were significantly lower compared to non-PVL. This difference was observed both in CIS patients (-7.9%, t = −4.9, p < 0.0001) and in RRMS patients (−7.7%, t = −9.14, p < 0.0001).

3.2. Band-wise analysis of MTR in periventricular normal-appearing white matter

The periventricular MTR values for all cohorts are summarized in Fig. 2A. A gradient is apparent even for HCs. Starting from the ventricle with lowest MTR values, MTR increased rapidly in the juxtaventricular area and became stable after a distance of 5 mm. This plateauing effect was also seen in CIS and RRMS. However, MS patients had significantly lower MTR values compared to HCs. Relative to HCs, the MTR-values were reduced up to 2.63% in CIS (at 4 mm distance, p < 0.0001) and 5.37% in RRMS (at 3 mm distance, p < 0.0001). Given differences in the female to male ratio between the groups (patients 2:1, HC 4:1), we also checked in the control group for a potential difference in mean MTR values per band by sex. However, there were no significant differences (data not shown). When considering the MTR relatively to the corresponding bands in HCs, both CIS and RRMS patients showed a strong gradient towards the ventricle, which was steeper in RRMS (Fig. 2B). The gradient became evident between the 3rd and last band. A linear regression revealed a relative MTR gradient of 0.18%/mm in CIS and 0.31%/mm in RRMS patients (see slopes in Fig. 2B). We have not found any association between band-wise MTR values in NAWM and age.

3.3. Association with cortical thickness

We first tested if MTR values in PVL and non-PVL were related to CMT. A positive association between MTR in PVL and CMT was found in CIS and RRMS patients (Fig. 3A), which was significant in RRMS (r_P = 0.28, p = 0.017), but not in CIS patients (r_P = 0.28, p = 0.094). No such association with CMT was observed for MTR values in non-PVL (RRMS: r_P = 0.038, p = 0.754; CIS: r_P = −0.162, p = 0.311) (Fig. 3B).

A correlation between the relative MTR gradient (relative to HCs) and CMT revealed a significant association in RRMS patients (r_P = -0.27, p = 0.020). A band-wise correlation revealed a significant relationship between periventricular MTR and CMT. As illustrated in Fig. 4A, we observed this relationship in almost all bands but it was strongest for the band next to the ventricle (r_P = 0.435, p = 0.0001; see scatterplot in Fig. 4C). No associations were found in HCs or CIS (data not shown).

3.4. Associations with disability

No significant associations were found between EDSS and normalized brain volume or normalized CMT. The total hyperintense WM-lesion volume was significantly associated with EDSS in RRMS (r_S = 0.314, p = 0.007), but this association was stronger for the PV lesion-load (r_S = 0.331, p = 0.005) than for the non-PV lesion-load (r_S = 0.222, p = 0.061). In contrast, CIS patients did not show a significant association for total hyperintense lesion-load (r_S = 0.066, p = 0.677), PV lesion-load (r_S = −0.001, p = 0.994) or non-PV lesion-load (r_S = −0.029, p = 0.856).

Lesional-MTR significantly correlated with EDSS, but only in PVL of RRMS patients (RRMS: r_P = −0.316, p = 0.007; CIS: r_P = −0.002, p = 0.992). The relative MTR gradient (relative to HCs) and EDSS were significantly correlated in RRMS patients (r_P = −0.31, p = 0.0077). Band-wise correlation of PV-MTR and EDSS (Fig. 4B) revealed significant associations in all bands. The correlation coefficient was highest in the first band and decreased with distance from the ventricle. The scatterplot corresponding to the correlation of PV-MTR values in the first band and EDSS is shown in Fig. 4D.

4. Discussion

In the current study, using multimodal MRI, we assessed periventricular tissue changes and related them to cortical thinning and clinical disability. We focused on focal T2-hyperintense lesions and microstructural tissue changes (assessed by means of the MTR), which allows a quantitative assessment of otherwise MRI invisible tissue damage (Enzinger and Fazekas, 2015; Granziera et al., 2021). To extend previous findings, we focused on early MS (i.e. after first clinical manifestation) to investigate how the MTR gradient around the ventricle relates to established MS with low disability and how much of this can be explained by periventricular tissue damage.

Extending previous MTR studies (Brown et al., 2020; 2017; Liu et al., 2015; Pardini et al., 2016; Poirion et al., 2021; Samson et al., 2014), we demonstrated that an abnormal gradient is present already at the earliest stage of the disease and that the steepness of the MTR gradient scales with clinical disability. This suggests that the accumulated tissue damage might be the consequence of a constant influx of CSF mediated factors that trigger inflammatory activity. Clearly, other and more globally acting pathophysiological mechanisms and partial volume

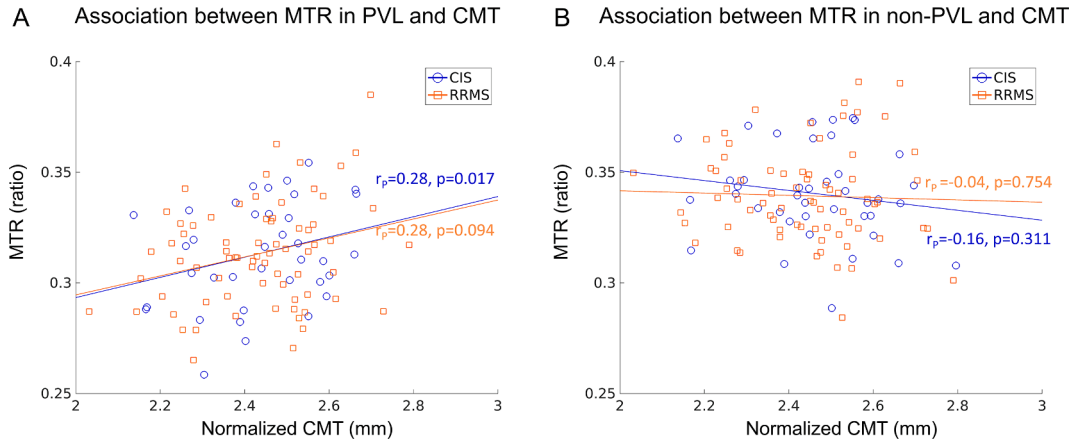

Fig. 3. ***A:*** Lower *MTR* values in periventricular lesions are significantly related to *reduced* cortical *thickness. This association was significant in RRMS and a trend was observed in CIS* (RRMS: r = 0.28, p = 0.017; CIS: r = 0.28, p = 0.094). ***B:*** No association was found in non-periventricular lesions (B) (RRMS: r = -0.038, p = 0.754; CIS: r = -0.162, p = 0.311) MTR = magnetisation transfer ratio, PVL = peri ventricular lesions, CMT = cortical mean thickness, CIS = clinically isolated syndrome, RRMS = relapsing-remitting multiple sclerosis.

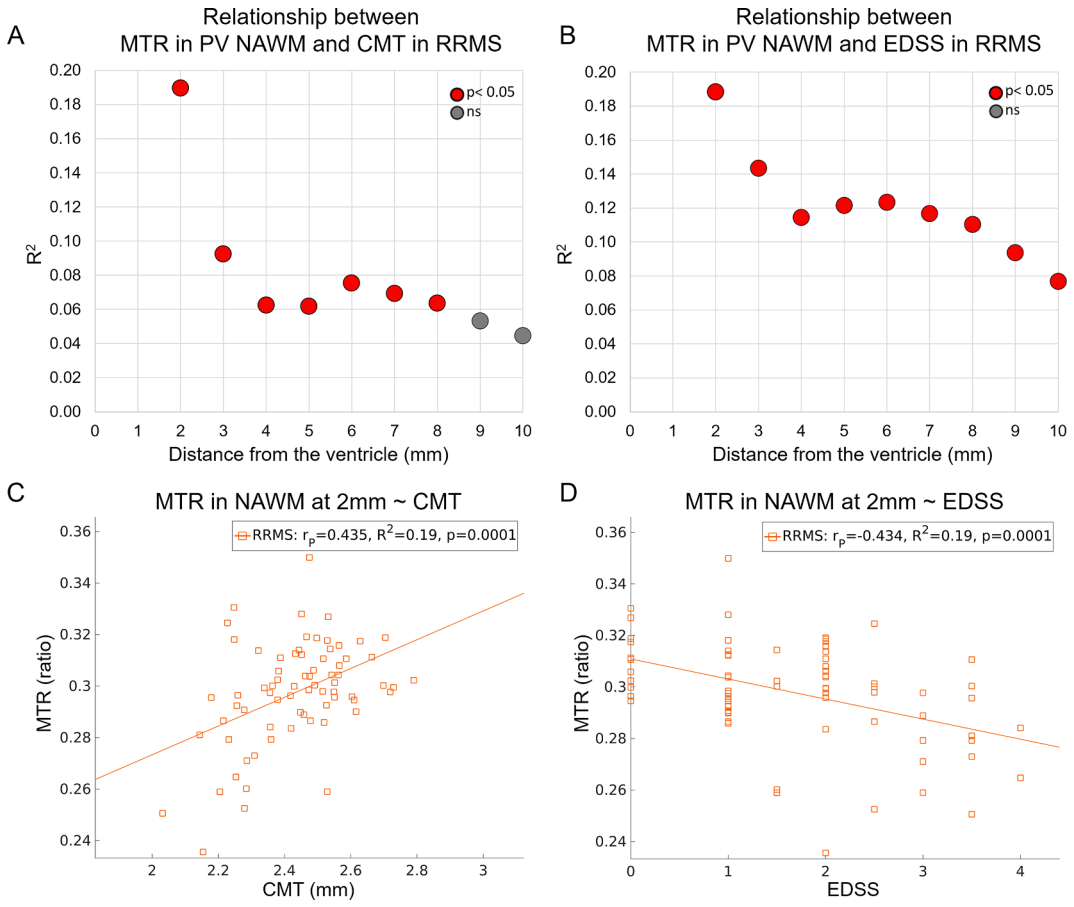

Fig. 4. **A:** Coefficient of correlation between cortical mean thickness (CMT) and MTR values in each periventricular band. Significant associations (indicated by the red filled circles) were found in RRMS but not in CIS patients. The strongest correlation coefficient (R^2) was found in the closest band to the ventricle. **B:** Coefficient of correlation of MTR values of each band with EDSS. MTR values in all bands were inversely correlated with EDSS, the strongest association was also found in the first band. **C:** Scatterplot of the association between MTR in NAWM at a distance of 2 mm from the ventricle and normalized CMT. **D:** Scatterplot showing the relation between MTR in NAWM at a distance of 2 mm from the ventricle and EDSS. R2 = coefficient of determination, ns = non-significant, MTR = magnetisation transfer ratio, NAWM = normal appearing white matter, PV = peri ventricular, CMT = (normalized) cortical mean thickness, RRMS = relapsing-remitting multiple sclerosis, EDSS = Expanded Disability Status Scale.

effects with CSF may also be responsible for local MTR variations. Supplementary to previous studies (Brown et al., 2020; 2017; Liu et al., 2015; Pardini et al., 2016; Poirion et al., 2021; Samson et al., 2014), we therefore also assessed cortical damage (evidenced by cortical thickness) and found a strong association between CMT and MTR in periventricular areas nearest to the CSF. Cortical thinning is already present in early disease stages (Calabrese et al., 2007) and has been associated with inflammation in histological post-mortem studies that showed T-cell infiltrates (Frischer et al., 2009) and B-cell follicle-like structures in the meninges. In these histological cases, a gradient-wise neuronal loss and meningeal inflammation starting from the outer cortical layers was observed.

The strong association between CMT and PV-MTR reductions supports the notion that common pathophysiologic mechanisms are shared at both sites (e.g., the penetration by CSF-mediated inflammatory infiltrates) and confirms its primary cause for the observed PV-MTR gradient. Further support results from the observation that highest correlation coefficients were found in bands nearest to the ventricles.

Indirect evidence for such a shared mechanism could also be demonstrated for PVL. Their MTR was lower than in non-PVL and also scaled with CMT, while non-PVL seemed to be decoupled from this process. We consider this evidence for CSF-induced MTR reductions in PVL as quite remarkable, as lesion pathology includes several processes including demyelination, gliosis, oligodendrocyte injury, neurodegeneration and axonal-loss, and also remyelination. Not all of them are directly related to inflammation and only some of them can be picked up with MT-imaging. PVL tend to occur around postcapillary veins and origin from an acute adaptive immune response (Absinta et al., 2016). Autoreactive and activated lymphocytes damage the blood–brain-barrier (BBB) of the postcapillary venules, which leads to increased permeability and eventually to dramatic structural disruption (Absinta et al., 2016; Zrzavy et al., 2017). The secretion of cytokines IFN-γ and tumour necrosis factor (TNF) by activated CD4 + lymphocytes upregulates endothelial adhesion molecules and chemokines, inducing a massive recruitment of monocyte-macrophages and allows the migration of these cells through the endothelium into the perivascular space and, subsequently, in the parenchyma. Matrix metalloproteinases have also been identified as potential factors, mediating the disruption of the BBB damaging endothelial tight junctions and basement membranes, and causing a leakage of water (vasogenic oedema) and serum proteins into WM (Absinta et al., 2016; Agrawal et al., 2013). Another potential contributor to the inflammatory demyelinating cascade might also be fibrin, which results from the impaired breakdown of leaking fibrinogen (Ryu et al., 2015). Together, this could also indicate a particular vulnerability of these regions to MS-related pathology.

The CSF-flow through the brain parenchyma follows the basement membranes between the outer pial coating of the artery and glia limitans (Engelhardt et al., 2016; Morris et al., 2016). Once the BBB is damaged, not only inflammatory cells in the serum but also soluble factors in the CSF might penetrate the PV-lesion and cause additional damage in the

lesion and in perilesional WM. The additional contribution of CSF soluble factors could explain the lower MTR values in PV-lesions compared to non-periventricular lesions. The diffusion of CSF factors through the ependyma might constitute a second pathway, because the ependyma might become more permeable as a consequence of inflammation (Adams et al., 1987). Evidence for increased PV inflammation in MS comes from a recent TSPO-PET study, demonstrating an increased immune cell activation in PVL and PV areas (Poirion et al., 2021). However, the pathophysiological correlate of the MTR reduction remains unclear. In WM, the MTR is commonly considered as a marker for myelin density and integrity (Barkhof et al., 2003; Moccia et al., 2020; Schmierer et al., 2010; 2004). To some degree, the MTR is also sensitive to microglia activation (Giannetti et al., 2015) and an increased water content (Vavasour et al., 2011), which may be induced by intrathecal inflammation and edema, but to a smaller extent (Dousset et al., 1992; Ropele et al., 2000; Stanisz et al., 2004). While a recent [^{18}F]-DPA714 PET study in progressive MS has demonstrated a gradient of innate immune-cell activation in PV-WM, it could not clarify the underlying mechanism for the MTR reduction. Therefore, longitudinal studies are needed to clarify if the MTR reflects just the inflammatory aspect or rather its microstructural consequence.

This study clearly confirms that PV-MTR abnormalities are already present in CIS patients suggestive of MS (i.e. with concomitant focal lesions on brain MRI) which recently has been shown in patients with optic-neuritis (Brown et al., 2017). When comparing the PV-MTR gradient with RRMS patients, a similar but flatter gradient was seen, suggesting that the same inflammatory process is shared. We were not able to demonstrate associations with cortical thickness and disability, but this may also be owed to the overall low EDSS score and the fact, that PV-MTR reductions reflect accumulated tissue damage rather than acute inflammatory processes.

Our study also has some limitations. The MTR sequence was not acquired at the same isotropic resolution as the T1-sequence, which was used for the ventricle segmentation and generation of periventricular bands. Therefore, application of registration and interpolation techniques were necessary. As the slice thickness of the MTR sequence was 3 mm, partial volume effects might have affected our analyses up to 3 mm distance from the ventricle. Within this distance, single voxels could still contain a significant amount of CSF, which might be the reason for the reduced MTR values in the initial bands in patients as well as HCs. Also, the initial relative MTR decrease in Fig. 2B might be attributed to partial volume effects and could explain why the gradient of relative MTR decrease became evident only after the 3rd band. An additional limitation might result from imperfect ventricle masks. However, since all ventricle masks have been assessed by visual inspection and all cohorts are affected to the same extent, we expect this bias to be neglectable. Furthermore, there were differences in the female to male ratio between the groups. However, while we are not aware of literature reporting sex-specific changes in PV areas, we specifically checked in the control group for a difference in mean MTR values per PV band by sex. As these analyses did not yield significant differences, a major confounding effect caused by sex cannot be expected. We could not investigate the possible impact of DAWM on the bandwise MTR analysis in this study, as no such cases were identified on FLAIR images. The absence of proton-density or T2-sequences may represent a limitation for identifying DAWM, however, DAWM induced MTR variations should have been visible on FLAIR images, because increased FLAIR intensities in dirty WM were equally related to increased T2 values (Maranzano et al., 2020).

In conclusion, our findings confirm the existence of a periventricular MTR-gradient in early MS. The MTR reduction indicates microstructural tissue damage and demyelination and becomes more pronounced in fully established MS. The association with cortical thinning in RRMS highlights the possibility of a shared inflammatory process due to CSF-mediated factors, which seem to exert a significant contribution to overall disease activity. Periventricular MTR can be measured in a robust and reproducible manner and might thus help to assess and monitor disease progression and treatment effects via multimodal MRI including refined regional analyses. Future work using longitudinal data with sufficiently long follow-up should also address the question whether the MTR-gradient may predict conversion from CIS into definite MS or even clinical worsening, i.e. investigate a potential predictive power.

CRediT authorship contribution statement

Lukas Pirpamer: Conceptualization, Methodology, Software, Formal analysis, Investigation, Data curation, Writing – original draft, Writing – review & editing, Visualization. **Bálint Kincses:** Formal analysis, Investigation, Data curation, Writing – original draft, Writing – review & editing, Visualization. **Zsigmond Tamás Kincses:** Conceptualization, Resources, Writing – review & editing. **Christian Kiss:** Resources, Writing – review & editing. **Anna Damulina:** Resources, Data curation. **Michael Khalil:** Resources, Data curation, Writing – review & editing. **Rudolf Stollberger:** Methodology. **Reinhold Schmidt:** Resources, Data curation, Writing – review & editing. **Christian Enzinger:** Conceptualization, Data curation, Project administration, Funding acquisition, Writing – original draft, Writing – review & editing. **Stefan Ropele:** Supervision, Conceptualization, Methodology, Resources, Writing – original draft, Writing – review & editing.

Declaration of Competing Interest

Part of this work (advanced MRI data analyses) has been supported and made possible by an unrestricted research grant by Sanofi-Aventis (project PM-ID 7851).

M.K. has received speaker honoraria from Bayer, Novartis, Merck, Biogen Idec and Teva Pharmaceutical Industries Ltd. and serves on scientific advisory boards for Biogen Idec, Merck Serono, Roche, Novartis, Bristol-Myers Squibb and Gilead. He received research grants from Teva Pharmaceutical Industries, Ltd., Biogen and Novartis.

C.E. received funding for traveling and speaker honoraria from Biogen Idec, Bayer Schering.

Pharma, Merck Serono, Novartis, Genzyme and Teva Pharmaceutical Industries Ltd./Sanofi-Aventis, Shire; received research support from Merck Serono, Biogen Idec, and Teva Pharmaceutical Industries Ltd./Sanofi-Aventis; and serves on scientific advisory boards for Bayer Schering Pharma, Biogen Idec, Merck Serono, Novartis, Genzyme, Roche, and Teva Pharmaceutical Industries Ltd./Sanofi- Aventis.

The remaining authors declare that they have no known competing financial interests or personal relationships that could have appeared to influence the work reported in this paper.

References:

Absinta, M., Sati, P., Reich, D.S., 2016. Advanced MRI and staging of multiple sclerosis lesions. Nat. Publ. Gr. 12, 358–368. https://doi.org/10.1038/nrneurol.2016.59.

Adams, C.W., Abdulla, Y.H., Torres, E.M., Poston, R.N., 1987. Periventricular lesions in multiple sclerosis: their perivenous origin and relationship to granular ependymitis. Neuropathol. Appl. Neurobiol. 13, 141–152. https://doi.org/10.1111/j.1365-2990.1987.tb00177.x.

Agrawal, S.M., Williamson, J., Sharma, R., Kebir, H., Patel, K., Prat, A., Wee Yong, V., 2013. Extracellular matrix metalloproteinase inducer shows active perivascular cuffs in multiple sclerosis. Brain 136, 1760–1777. https://doi.org/10.1093/brain/awt093.

Barkhof, F., Brück, W., De Groot, C.J.A., Bergers, E., Hulshof, S., Geurts, J., Polman, C.H., Van der Valk, P., 2003. Remyelinated lesions in multiple sclerosis: magnetic resonance image appearance. Arch. Neurol. 60, 1073–1081. https://doi.org/10.1001/archneur.60.8.1073.

Brown, J.W.L., Pardini, M., Brownlee, W.J., Fernando, K., Samson, R.S., Carrasco, F.P., Ourselin, S., Gandini Wheeler-Kingshott, C.A.M., Miller, D.H., Chard, D.T., 2017. An abnormal periventricular magnetization transfer ratio gradient occurs early in multiple sclerosis. Brain 140, 387–398. https://doi.org/10.1093/brain/aww296.

Brown, J.W.L., Prados Carrasco, F., Eshaghi, A., Sudre, C.H., Button, T., Pardini, M., Samson, R.S., Ourselin, S., Wheeler-Kingshott, C.A.G., Jones, J.L., Coles, A.J., Chard, D.T., 2020. Periventricular magnetisation transfer ratio abnormalities in multiple sclerosis improve after alemtuzumab. Mult. Scler. J. 26, 1093–1101. https://doi.org/10.1177/1352458519852093.

Calabrese, M., Atzori, M., Bernardi, V., Morra, A., Romualdi, C., Rinaldi, L., McAuliffe, M.J.M., Barachino, L., Perini, P., Fischl, B., Battistin, L., Gallo, P., 2007. Cortical atrophy is relevant in multiple sclerosis at clinical onset. J. Neurol. 254, 1212–1220. https://doi.org/10.1007/s00415-006-0503-6.

Dousset, V., Grossman, R.I., Ramer, K.N., Schnall, M.D., Young, L.H., Gonzalez-Scarano, F., Lavi, E., Cohen, J.A., 1992. Experimental allergic encephalomyelitis and multiple sclerosis: lesion characterization with magnetization transfer imaging. Radiology 182, 483–491. https://doi.org/10.1148/radiology.182.2.1732968.

Engelhardt, B., Carare, R.O., Bechmann, I., Flügel, A., Laman, J.D., Weller, R.O., 2016. Vascular, glial, and lymphatic immune gateways of the central nervous system. Acta Neuropathol. 132, 317–338. https://doi.org/10.1007/s00401-016-1606-5.

Enzinger, C., Fazekas, F., 2015. Measuring gray matter and white matter damage in MS: why this is not enough. Front. Neurol. 6, 1–4. https://doi.org/10.3389/fneur.2015.00056.

Filippi, M., Campi, A., Dousset, V., Baratti, C., Martinelli, V., Canal, N., Scotti, G., Comi, G., 1995. A magnetization transfer imaging study of normal-appearing white matter in multiple sclerosis. Neurology 45, 478–482. https://doi.org/10.1212/WNL.45.3.478.

Frischer, J.M., Bramow, S., Dal-Bianco, A., Lucchinetti, C.F., Rauschka, H., Schmidbauer, M., Laursen, H., Sorensen, P.S., Lassmann, H., 2009. The relation between inflammation and neurodegeneration in multiple sclerosis brains. Brain 132, 1175–1189. https://doi.org/10.1093/brain/awp070.

Giannetti, P., Politis, M., Su, P., Turkheimer, F.E., Malik, O., Keihaninejad, S., Wu, K., Waldman, A., Reynolds, R., Nicholas, R., Piccini, P., 2015. Increased PK11195-PET binding in normal-appearing white matter in clinically isolated syndrome. Brain 138, 110–119. https://doi.org/10.1093/brain/awu331.

Granziera, C., Wuerfel, J., Barkhof, Frederik, Calabrese, M., De Stefano, Nicola, Enzinger, Christian, Evangelou, N., Filippi, Massimo, Geurts, J.J.G., Reich, D.S., Rocca, Maria A, Ropele, S., Rovira, Àlex, Sati, P., Toosy, A.T., Vrenken, Hugo, Gandini Wheeler-Kingshott, C.A.M., Kappos, Ludwig, Barkhof, F, de Stefano, N, Sastre-Garriga, J., Ciccarelli, O., Enzinger, C, Filippi, M, Gasperini, C., Kappos, L, Palace, J., Vrenken, H, Rovira, À, Rocca, M A, Yousry, T., 2021. Quantitative magnetic resonance imaging towards clinical application in multiple sclerosis. Brain 144, 1296–1311. https://doi.org/10.1093/brain/awab029.

Jehna, M., Pirpamer, L., Khalil, M., Fuchs, S., Ropele, S., Langkammer, C., Pichler, A., Stulnig, F., Deutschmann, H., Fazekas, F., Enzinger, C., 2015. Periventricular lesions correlate with cortical thinning in multiple sclerosis. Ann. Neurol. 78 (4), 530–539.

Kurtzke, J.F., 1983. Rating neurologic impairment in multiple sclerosis: an expanded disability status scale (EDSS). Neurology 33, 1444. https://doi.org/10.1212/WNL.33.11.1444.

Lassmann, H., 2014. Multiple sclerosis: lessons from molecular neuropathology. Exp. Neurol. 262, 2–7. https://doi.org/10.1016/j.expneurol.2013.12.003.

Liu, Z., Pardini, M., Yaldizli, Ö., Sethi, V., Muhlert, N., Wheeler-Kingshott, C.A.M., Samson, R.S., Miller, D.H., Chard, D.T., 2015. Magnetization transfer ratio measures in normal-appearing white matter show periventricular gradient abnormalities in multiple sclerosis. Brain 138, 1239–1246. https://doi.org/10.1093/brain/awv065.

Magliozzi, R., Howell, O.W., Reeves, C., Roncaroli, F., Nicholas, R., Serafini, B., Aloisi, F., Reynolds, R., 2010. A Gradient of neuronal loss and meningeal inflammation in multiple sclerosis. Ann. Neurol. 68, 477–493. https://doi.org/10.1002/ana.22230.

Maranzano, J., Dadar, M., Zhernovaia, M., Arnold, D.L., Collins, D.L., Narayanan, S., 2020. Automated separation of diffusely abnormal white matter from focal white matter lesions on MRI in multiple sclerosis. Neuroimage 213, 116690. https://doi.org/10.1016/j.neuroimage.2020.116690.

Moccia, M., van de Pavert, S., Eshaghi, A., Haider, L., Pichat, J., Yiannakas, M., Ourselin, S., Wang, Y., Wheeler-Kingshott, C., Thompson, A., Barkhof, F., Ciccarelli, O., 2020. Pathologic correlates of the magnetization transfer ratio in multiple sclerosis. Neurology 95 (22), e2965–e2976.

Morris, A.W.J., Sharp, M.M.G., Albargothy, N.J., Fernandes, R., Hawkes, C.A., Verma, A., Weller, R.O., Carare, R.O., 2016. Vascular basement membranes as pathways for the passage of fluid into and out of the brain. Acta Neuropathol. 131, 725–736. https://doi.org/10.1007/s00401-016-1555-z.

Pardini, M., Sudre, C.H., Prados, F., Yaldizli, Ö., Sethi, V., Muhlert, N., Samson, R.S., Van De Pavert, S.H., Cardoso, M.J., Ourselin, S., Gandini Wheeler-Kingshott, C.A.M., Miller, D.H., Chard, D.T., 2016. Relationship of grey and white matter abnormalities with distance from the surface of the brain in multiple sclerosis. J. Neurol. Neurosurg. Psychiatry 87, 1212–1217. https://doi.org/10.1136/jnnp-2016-313979.

Poirion, E., Tonietto, M., Lejeune, F.X., Ricigliano, V.A.G., Boudot de la Motte, M., Benoit, C., Bera, G., Kuhnast, B., Bottlaender, M., Bodini, B., Stankoff, B., 2021. Structural and clinical correlates of a periventricular gradient of neuroinflammation in multiple sclerosis. Neurology 96, e1865–e1875. https://doi.org/10.1212/WNL.0000000000011700.

Polman, C.H., Reingold, S.C., Banwell, B., Clanet, M., Cohen, J.A., Filippi, M., Fujihara, K., Havrdova, E., Hutchinson, M., Kappos, L., Lublin, F.D., Montalban, X., O'Connor, P., Sandberg-Wollheim, M., Thompson, A.J., Waubant, E., Weinshenker, B., Wolinsky, J.S., 2011. Diagnostic criteria for multiple sclerosis: 2010 Revisions to the McDonald criteria. Ann. Neurol. 69, 292–302. https://doi.org/10.1002/ana.22366.

Ropele, S., Fazekas, F., 2009. Magnetization transfer MR imaging in multiple sclerosis. Neuroimaging Clin. N. Am. 19, 27–36. https://doi.org/10.1016/j.nic.2008.09.004.

Ropele, S., Strasser-Fuchs, S., Augustin, M., Stollberger, R., Enzinger, C., Hartung, H.P., Fazekas, F., 2000. A comparison of magnetization transfer ratio, magnetization transfer rate, and the native relaxation time of water protons related to relapsing-remitting multiple sclerosis. AJNR. Am. J. Neuroradiol. 21, 1885–1891.

Ryu, J.K., Petersen, M.A., Murray, S.G., Baeten, K.M., Meyer-Franke, A., Chan, J.P., Vagena, E., Bedard, C., Machado, M.R., Coronado, P.E.R., Prod'homme, T., Charo, I. F., Lassmann, H., Degen, J.L., Zamvil, S.S., Akassoglou, K., 2015. Blood coagulation protein fibrinogen promotes autoimmunity and demyelination via chemokine release and antigen presentation. Nat. Commun. 6 (1) https://doi.org/10.1038/ncomms9164.

Samson, R.S., Cardoso, M.J., Muhlert, N., Sethi, V., Wheeler-Kingshott, C.A.M., Ron, M., Ourselin, S., Miller, D.H., Chard, D.T., 2014. Investigation of outer cortical magnetisation transfer ratio abnormalities in multiple sclerosis clinical subgroups. Mult. Scler. 20, 1322–1330. https://doi.org/10.1177/1352458514522537.

Schmierer, K., Parkes, H.G., So, P.W., An, S.F., Brandner, S., Ordidge, R.J., Yousry, T.A., Miller, D.H., 2010. High field (9.4 Tesla) magnetic resonance imaging of cortical grey matter lesions in multiple sclerosis. Brain 133, 858–867. https://doi.org/10.1093/brain/awp335.

Schmierer, K., Scaravilli, F., Altmann, D.R., Barker, G.J., Miller, D.H., 2004. Magnetization transfer ratio and myelin in postmortem multiple sclerosis brain. Ann. Neurol. 56 (3), 407–415.

Serafini, B., Rosicarelli, B., Magliozzi, R., Stigliano, E., Aloisi, F., 2004. Detection of ectopic B-cell follicles with germinal centers in the meninges of patients with secondary progressive multiple sclerosis. Brain Pathol. 14, 164–174. https://doi.org/10.1111/j.1750-3639.2004.tb00049.x.

Stanisz, G.J., Webb, S., Munro, C.A., Pun, T., Midha, R., 2004. MR properties of excised neural tissue following experimentally induced inflammation. Magn. Reson. Med. 51 (3), 473–479.

Storch, M.K., Bauer, J., Linington, C., Olsson, T., Weissert, R., Lassmann, H., 2006. Cortical demyelination can be modeled in specific rat models of autoimmune encephalomyelitis and is Major Histocompatability Complex (MHC) haplotype-related. J. Neuropathol. Exp. Neurol. 65, 1137–1142. https://doi.org/10.1097/01.jnen.0000248547.13176.9d.

Vavasour, I.M., Laule, C., Li, D.K.B.B., Traboulsee, A.L., MacKay, A.L., 2011. Is the magnetization transfer ratio a marker for myelin in multiple sclerosis? J. Magn. Reson. Imaging 33, 710–718. https://doi.org/10.1002/jmri.22441.

Zrzavy, T., Hametner, S., Wimmer, I., Butovsky, O., Weiner, H.L., Lassmann, H., 2017. Loss of "homeostatic" microglia and patterns of their activation in active multiple sclerosis. Brain 140, 1900–1913. https://doi.org/10.1093/brain/awx113.